Title
Krüppel Mediates the Selective Rebalancing of Ion Channel Expression

Permalink
https://escholarship.org/uc/item/3jh1x10m

Authors
Parrish, Jay Z
Kim, Charles C
Tang, Lamont
et al.

Peer reviewed

Krüppel Mediates the Selective Rebalancing of Ion Channel Expression

Jay Z. Parrish[1,6,*], **Charles C. Kim**[2,6,*], **Lamont Tang**[3], **Sharon Bergquist**[3], **Tingting Wang**[3], **Joseph L. DeRisi**[3,4], **Lily Yeh Jan**[3,4,5], **Yuh Nung Jan**[3,4,5], and **Graeme W. Davis**[3,*]

[1]Department of Biology, University of Washington, Seattle, WA 98195, USA

[2]Division of Experimental Medicine, Department of Medicine, University of California, San Francisco, San Francisco, CA 94110, USA

[3]Department of Biochemistry and Biophysics, University of California, San Francisco, San Francisco, CA 94158, USA

[4]Howard Hughes Medical Institute, University of California, San Francisco, San Francisco, CA 94158, USA

[5]Department of Physiology, University of California, San Francisco, San Francisco, CA 94158, USA

SUMMARY

Ion channel gene expression can vary substantially among neurons of a given type, even though neuron-type-specific firing properties remain stable and reproducible. The mechanisms that modulate ion channel gene expression and stabilize neural firing properties are unknown. In *Drosophila*, we demonstrate that loss of the *Shal* potassium channel induces the compensatory rebalancing of ion channel expression including, but not limited to, the enhanced expression and function of *Shaker* and *slowpoke*. Using genomic and network modeling approaches combined with genetic and electrophysiological assays, we demonstrate that the transcription factor *Krüppel* is necessary for the homeostatic modulation of *Shaker* and *slowpoke* expression. Remarkably, *Krüppel* induction is specific to the loss of *Shal*, not being observed in five other potassium channel mutants that cause enhanced neuronal excitability. Thus, homeostatic signaling systems responsible for rebalancing ion channel expression can be selectively induced after the loss or impairment of a specific ion channel.

*Correspondence: jzp2@uw.edu (J.Z.P.), charlie.kim@ucsf.edu (C.C.K.), graeme.davis@ucsf.edu (G.W.D.).
[6]Co-first author

INTRODUCTION

The nervous system is continually modified by experience. Given the tremendous complexity of the nervous system, it is astounding that robust and reproducible neural function can be sustained throughout life. It is now apparent that homeostatic signaling systems stabilize the function of nerve and muscle and, thereby, constrain how the nervous system can be altered by experience or crippled by disease (Davis, 2006; Marder and Goaillard, 2006; Ramocki and Zoghbi, 2008; Turrigiano and Nelson, 2004).

The homeostatic control of ion channel gene expression has been documented in experimental systems as diverse as the mammalian hippocampus (Nerbonne et al., 2008), lobster stomatogastric ganglion (MacLean et al., 2005), and the *Drosophila* neuromuscular system (Bergquist et al., 2010). In each instance, the loss or misexpression of an ion channel gene induces a compensatory change in the expression of related channels that largely restore appropriate neuronal firing properties. Defining the molecular basis of these compensatory signaling systems may have broad implications for our understanding and treatment of diseases that are characterized by the aberrant function of neural circuitry including autism (Ramocki and Zoghbi, 2008) and epilepsy (Houweling et al., 2005). To date, the molecular mechanisms underlying this powerful form of neuronal regulation remain virtually unknown (Dulcis et al., 2013; Spitzer, 2012; Temporal et al., 2012).

We have used *Drosophila* to identify a molecular mechanism that participates in the homeostatic control of potassium channel gene expression. In *Drosophila* motoneurons, loss of the Kv4.2 ortholog *Shal* initiates a compensatory increase in the expression of *Shaker* (*Sh*), which encodes a functionally similar A-type potassium channel (Bergquist et al., 2010; Figure S1 available online). Here, we sought to identify the mechanism responsible for the compensatory transcriptional modulation of *Sh* gene expression. We identify Krüppel (Kr) as a central regulator of this process and provide evidence that the compensatory response includes ion channels in addition to *Sh*. Remarkably, Kr itself is only responsive to the loss of the *Shal* potassium channel and is not induced in animals that harbor mutations in other ion channel genes that cause similar neuronal hyperactivity. As such, our data suggest the existence of selective signaling systems that couple specific ion channels to compensatory transcription factor-based homeostatic signaling in the neuronal nucleus.

RESULTS AND DISCUSSION

For our studies, we began with two underlying hypotheses. First, the transcription factors that developmentally control *Sh* expression levels will also be responsible for the homeostatic modulation of *Sh* expression. Second, relevant transcription factors will be upregulated in the *Shal* mutant compared to wild-type.

To identify factors involved in homeostatic control of ion channel expression, we combined expression profiling of neurons with regulatory network modeling. Using FACS, we isolated specific cell types followed by gene expression analysis with *Drosophila* microarrays. The data revealed a rich pattern of regulation including cell-type-specific changes in gene expression over larval development (Figure 1A). To validate the robustness of the data, we

performed an unbiased comparison to gene expression patterns in the Berkeley *Drosophila* Genome Project (BDGP) in situ hybridization database (Tomancak et al., 2002). We calculated the mean microarray expression value of all genes in each BDGP anatomical category for each FACS-isolated population, as well as the significance of the expression value based on an empirically derived random model. We observed striking concordance in gene expression patterns between the BDGP in situ database and our data (Figure 1B), demonstrating robustness in both. Consistent with RNA sequencing profiles of whole larvae (Marygold et al., 2013), sorted neuronal populations exhibit pronounced changes during larval development in the expression of ion channels and transcription factors (Table S1), allowing for the identification of transcription factors that developmentally covary with ion channel expression.

To identify candidate transcription factors that regulate ion channel expression, we generated a regulatory network model (Margolin et al., 2006). In this approach, covariance is quantified by pairwise mutual information of genes across all samples. Insignificant and indirect interactions are eliminated, resulting in a model enriched in direct regulatory interactions. A subnetwork including only genes encoding channels and transcription factors, as annotated in FlyBase (Marygold et al., 2013) and FlyTF.org (Adryan and Teichmann, 2006), respectively, was used to identify transcription factors predicted to control ion channel expression (Figure S2). In this subnetwork, *Kr* is among a small number of transcription factors that are directly linked to *Sh* (Figure 1C and Figure S2), making it a candidate regulator of *Sh* expression. *Kr* encodes one of the founding members of the Krüppel-like factor (KLF) family of transcription factors that regulate proliferation and differentiation and are master regulators of cell fate in many tissues in both invertebrates and vertebrates (Hoch and Jäckle, 1998; Isshiki et al., 2001; Jiang et al., 2008; Moore et al., 2009).

Next, we conducted whole-genome expression analysis of wild-type and *Shal^495^* null mutant motoneurons isolated from third-instar *Drosophila* larvae (Table S2). Using this approach we find that both *Kr* and *Sh* are upregulated in *Shal* mutant motoneurons (Figures 1D and 1E). Kr is, thus, one of only three transcription factors identified as candidate regulators of *Sh* by both developmental regulatory network modeling and *Shal* disruption. In addition to *Sh*, 19 ion channel-encoding genes are differentially regulated after loss of *Shal* (Figure 1D). Among the upregulated genes is *gfA*, an acetylcholine receptor subunit recently shown to be transcriptionally coupled to *Shal* by an unknown mechanism (Ping and Tsunoda, 2012). Both depolarizing and hyperpolarizing channels are altered in *Shal^495^*, representing a more complex genomic response than previously appreciated (Bergquist et al., 2010; MacLean et al., 2005; Nerbonne et al., 2008). The *Shal^495^* mutation is a protein null. However, we note that some nontranslated transcripts are upregulated in this mutant, an observation that could indicate homeostatic feedback to the *Shal* locus or an unknown molecular response to the presence of the *Shal^495^* mutation. Here, we pursue the hypothesis that *Kr* mediates the compensatory change in *Sh* gene expression, which we have previously demonstrated to have functional relevance in vivo (Bergquist et al., 2010).

To test whether increased levels of *Kr* might be responsible for the increase in *Sh* expression caused by loss of *Shal*, we asked whether *Kr* overexpression is sufficient to increase the

expression of *Sh*. This is what we observe (Figures 1F and 1G; Table S3). *Kr* overexpression also increases the expression of 17 other ion channel genes including I_h and the potassium channel *slowpoke* (*slo*). Importantly, both *slo* and I_h are also upregulated in *Shal*[495] mutant motoneurons, along with *Sh*. Thus, *Kr* overexpression is able to drive the increase in expression of *Sh*, *slo*, and I_h after loss of *Shal*. We also note that several transcription factors are similarly altered when we compare the motoneuron transcriptional response to loss of *Shal* function and *Kr* overexpression (Figure 1G). This is consistent with *Kr* controlling a regulatory hierarchy, ultimately leading to changes in ion channel gene expression.

We next confirmed that Kr protein is regulated by loss of *Shal*. In the late-stage embryo, *Kr* transcript and Kr protein are expressed throughout the nervous system (Figures 2A and 2B). As development proceeds, *Kr* expression diminishes and Kr protein is nearly absent from the third-instar CNS (Figure 2C, left). However, in *Shal* mutants, high levels of Kr protein are observed in the third-instar CNS (Figure 2C, right). This was confirmed by qPCR (Figure 2D) and in situ hybridization (data not shown). Thus, *Kr* transcript and protein levels are increased after loss of *Shal*.

We considered two models for the induction of *Kr* expression after loss of *Shal*. In one model, increased neural activity, caused by loss of *Shal*, drives the change in *Kr* expression. An alternative model is that *Kr* expression is specifically coupled to loss of the channel encoded by *Shal*, irrespective of altered neural activity. To distinguish between these possibilities, we examined five additional potassium channel mutants, each of which causes hyperexcitability in motoneurons. Remarkably, *Kr* transcript and protein were substantially increased only in the *Shal* mutant (Figures 2D and 2E, respectively). We observed no change in *Kr* mRNA in a sodium channel mutant (*para*[1]), a calcium channel mutant (*cac*[1]), or a series of potassium channel mutants (*Shab*[f05893], *Shawl*[f04377], *slo*[1], *eag*[1], and *Hk*[1]) and only a minor increase in Kr protein in *para* mutants. We conclude that increased *Kr* expression is linked to the loss of *Shal*, rather than a general increase in neural activity. These data suggest remarkable specificity within the homeostatic signaling system that controls potassium channel gene expression.

We next asked whether *Kr* expression is induced by loss of the Shal channel conductance. Since *Kr* responds only to the loss of *Shal*, not *Sh* (Figures 2D and 2E), we reasoned that 4-aminopyridine (4-AP), which inhibits Shal and Sh potassium channels, would induce *Kr* expression as a result of Shal channel inhibition. Larvae were fed 4-AP in yeast paste for either 18 or 24 hr and compared to controls that received yeast paste without 4-AP. Animals fed 4-AP exhibited a significant increase in the number of Kr-expressing cells in the CNS compared to controls (Figures 2F and 2G), demonstrating that Kr expression is sensitive to loss of the Shal conductance. By extension, these data also suggest the existence of mechanisms capable of detecting loss of the Shal conductance, rather than simply the presence or absence of the Shal protein or transcript.

Next, we sought to determine whether *Kr* is necessary in motoneurons for a functional increase in Sh activity. Sh protein is localized to the axon and nerve terminal, making it impossible to directly assay the Sh current through somatic recordings (Bergquist et al., 2010). Additionally, available antibodies do not detect Sh protein in situ. To assess Sh

expression, we therefore utilized an assay that allows us to report Sh activity through its influence on synaptic transmission at the nerve terminal (Figure S1). Specifically, increased Sh within the axon and nerve terminal completely occludes the enhancement of presynaptic neurotransmitter release that occurs after inhibition of postsynaptic glutamate receptors (synaptic homeostasis [Bergquist et al., 2010]). Here, we confirm that this effect is also achieved by neuronal *Shal* knockdown. In wild-type animals, application of the glutamate receptor antagonist philanthotoxin 433 (PhTx) decreases miniature excitatory postsynaptic potential (mEPSP) amplitudes and induces a corresponding increase in presynaptic release (quantal content; Figures 3A–3C, black). The increase in quantal content is blocked in animals neuronally expressing *Shal-RNAi* (Figures 3A–3C, red). Upon simultaneous neuronal expression of *UAS-Kr-RNAi* with *Shal-RNAi* (postembryonically), synaptic homeostasis is restored (Figures 3A–3C, blue). This result is consistent with *Kr* being necessary for increased expression of *Sh* after loss of *Shal*. To further support this conclusion, we asked whether *Kr* overexpression, which is sufficient to drive *Sh* expression, also occludes synaptic homeostasis. This is what we observe (Figures 3E and 3F). Finally, the occlusion of synaptic homeostasis caused by expression of *UAS-Kr* is largely reversed when we coexpress *UAS-Kr* with *UAS-Sh-RNAi* to prevent an increase in *Sh* expression (Figures 3E and 3F). Taken together, these data provide evidence that *Kr* is both necessary for a functional increase in *Sh* expression, in motoneurons, caused by loss of *Shal*, and, when overexpressed, is able to induce the observed changes in *Sh* expression.

We next addressed whether Sh is the only channel downstream of Kr that participates in the homeostatic rebalancing of ion channel expression. Data from other systems indicate that multiple channels can participate in this type of response (Nerbonne et al., 2008). Our genomic analyses demonstrate that *slo* is upregulated in both *Shal* mutants and after *Kr* overexpression, providing an opportunity to test the involvement of another channel. At the *Drosophila* NMJ, Slo channels are present presynaptically and participate in action potential repolarization along with Sh (Gho and Ganetzky, 1992). To determine whether Slo contributes to the *Kr*-dependent rebalancing of ion channel expression, we performed experiments identical to those described above. The slo^1 mutation does not alter baseline quantal content (data not shown). However, when the slo^1 mutant is placed in the background of either *Shal-RNAi* or *Kr* overexpression, homeostatic plasticity is restored (Figures 3G and 3H). We note that statistically significant homeostatic potentiation is observed when either Slo or Shaker is removed in the *Shal* or *Kr* overexpression backgrounds. But removal of each channel alone does not allow homeostatic synaptic potentiation to reach wild-type levels, consistent with both channels being upregulated and functionally important after loss of *Shal* (Figures 3H and 3F). These data demonstrate that *Kr*-dependent ion channel rebalancing includes the modulation of Slo expression. Thus, Kr appears to control a complex homeostatic response involving at least Slo and Shaker, consistent with the complexity of such ion channel rebalancing in other systems (Nerbonne et al., 2008).

Finally, we asked whether this signaling system is generally applicable to other neuronal types. *Kr* expression is developmentally regulated in PNS neurons (Figures 4A and 4B) and Kr protein is detectable in embryonic but not larval PNS neurons (Figures 4A and 4B). As in

the CNS, Kr protein is significantly increased in the larval PNS of *Shal* mutants (Figure 4B, right) and ectopic *Kr* expression is sufficient to drive increased *Sh* expression (Figure 4C; Table S4). Notably, there is considerable overlap in *Kr*-induced channels in the PNS and CNS, including *SK*, *Shaw*, *Ca-alpha1T*, *Teh1*, *Sh*, *brp*, *nAcRalpha-30D*, *cac*, *slo*, *GluClalpha*, *Ih*, and *pHCl*. Thus, *Kr* expression and the downstream transcriptional control of ion channel expression may be a generalized signaling system in diverse neuronal types.

In summary, we provide evidence that the cell fate regulator Kr is a critical player in the compensatory control of potassium channel gene expression. We speculate that the induction of *Kr* drives a pattern of gene expression, first used to establish neuronal identity in the embryo and then, postembryonically, to rebalance ion channel expression in the face of persistent or acute perturbation of the *Shal* channel. Surprisingly, *Kr* is induced after the loss of *Shal*, but not other potassium channel gene mutations that have been shown to cause neural hyperexcitability. We conclude that Shal function is specifically coupled to a homeostatic feedback system that includes the *Kr*-dependent transcriptional response. As such, these data imply the existence of discoverable "rules" that define how individual neurons will respond to mutations in ion channel genes.

Recent work underscores the possibility that the regulation of ion channel expression can be conserved from *Drosophila* to mammalian central neurons. In *Drosophila*, the translational regulator Pumilio was shown to be necessary and sufficient for the modulation of sodium channel transcription after persistent changes to synaptic transmission in the CNS (Mee et al., 2004; Muraro et al., 2008). More recent data indicate that Pumilio-2 regulates NaV1.6 translation in rat visual cortical pyramidal neurons in a manner consistent with that observed in *Drosophila* (Driscoll et al., 2013). In mammalian neurons, *Kr-like* genes (*KLF*) respond to neuronal activity (Scobie et al., 2009) and are studied intensively in the context of axonal regeneration (Moore et al., 2009), but a role in ion channel expression or homeostatic rebalancing has yet to be defined.

Kr and its homologs are potent regulators of neuronal cell fate. KLF4 and KLF5, in particular, have been shown to both maintain and reprogram embryonic stem cell fate (Sur, 2009). We provide evidence that Kr protein levels diminish to nearly undetectable levels in the postembryonic CNS. Kr expression is then induced to achieve potassium channel regulation. It is tempting to speculate that the rebalancing of ion channel expression postembryonically is a reinduction of the embryonic mechanisms that initially specify neuronal active properties.

EXPERIMENTAL PROCEDURES

Fly Stocks

The following alleles were used in this study: w^{118}, $gal4^{C155}$ *(elav-Gal4)*, *elav-Gal4 (III)*, *OK371-Gal4*, *RN2-Gal4*, *21-7-Gal4*, *UAS-mCD8-GFP*, *UASt2GFP*, mhc^{weep}, arm^{weep}, *ppk-eGFP*, *3xppk-mCD8-GFP*, *UAS-TnT*, *UASKir*, *UAS-Kr*, *UAS-Shal-RNAi*, *UAS-Kr-RNAi*, *UAS-Sh-RNAi*, $Shal^{495}$, Sh^{14}, Hk^1, $para^1$, slo^1, cac^1, eag^1, $Shawl^{f04377}$, and $Shab^{f05893}$. Detailed descriptions of each allele are available at flybase: http://www.flybase.org.

Cell Dissociation

20–24 hr Samples—For all samples except *Arm::GFP*, late-stage embryos were dechorionated in 50% bleach, washed extensively in PBS, and resuspended in approximately 5 vol of PBS/2x trypsin (Life Technologies). Embryos were homogenized with 15 strokes of a Dounce homogenizer, followed by three cycles of the following: mixing 5 min at 1,000 rpm in 37°C microtube mixer and triturating by pipetting ten times through a 200 ml pipet tip. For *Arm::GFP* samples, individual embryos were dissected using a tungsten needle (FST) prior to trypsinization to isolate body wall epithelium from other tissues labeled by *Arm::GFP*.

Larval Samples—For all other time points, larvae were filleted in PBS and the tissue containing cells of interest was dissected away from all other tissues. For body wall samples (muscle, epithelia, and peripheral nervous system [PNS] neurons), care was taken to completely remove imaginal discs and the brain/ventral nerve cord (VNC), both to reduce the complexity of cell suspensions for fluorescence-activated cell sorting (FACS) and to remove possible contaminants. For PNS-md samples, the thoracic segments of the body wall were dissected away as *Gal4^21-7* labels a small number of epithelia cells in these segments. For CNS samples, larval brains were dissected away from all other tissue prior to dissociation. Dissection time was limited to 30 min for each sample, and after dissection cell suspensions were prepared in 5 vol of PBS/2x trypsin via three cycles of the following: triturate ten times through a pipet tip (P1000 tip for body wall samples, P200 tip for CNS samples), mix 5 min at 1,000 rpm in a 37°C microtube mixer.

FACS Isolation

After dissociation, samples were filtered through a 70 μm cell strainer and sorted on a FACSAria or FACSAria II (Becton Dickinson). Neuronal and epithelial populations exhibited different forward scatter (FSC) and side scatter (SSC) properties, which increased gating specificity. GFP⁺ nonautofluorescent events were sorted into 100 μl RNAqueous-Micro Lysis buffer (Life Technologies), and samples were immediately frozen on dry ice.

Microarray Design

We designed two 60-mer oligonucleotide probes for each of the 20,726 coding sequences in the annotated fly genome (release 5.2) using ArrayOligoSelector (Bozdech et al., 2003), resulting in 35,272 successful probe designs, 16,717 additional probes against alternatively spliced transcripts, and 546 probes targeting noncoding RNA (244 snoRNA, 108 tRNA, 24 snRNA, 74 rRNA, 3 miRNA, and 93 other). The final probe set was filtered to remove redundant probes, overlapping probes, and those with cross-hybridization potential (based on a −21.6 kcal/mol threshold, which was chosen to fit the number of probes allowed in the Agilent 4 × 44k design specification). This resulted in 33,792 probes to CDS, 8,744 probes to alternatively spliced transcripts, and 546 RNA probes. In total, 43,803 probes were included in the design.

RNA Isolation, Amplification, and Microarray Hybridization

RNA was isolated from FACS-sorted samples using the RNAqueous-Micro kit and DNase treated as per the manufacturer's recommendations. All RNA samples were subjected to two rounds of linear amplification using the Aminoallyl MessageAmp II kit (Life Technologies). Dye-coupled aRNA was fragmented and hybridized to custom-designed microarrays as per the manufacturer recommendations (Agilent Technologies).

Microarray Scanning, Feature Extraction, Normalization, and Filtering

Microarrays were scanned on an Axon 4000B scanner and feature information extracted in GenePix 6 (Molecular Devices). GPR files were uploaded into Acuity (Molecular Devices) and ratio normalized. Data were retrieved using quality filters for reference channel intensity, background intensity, pixel saturation, pixel variance, feature diameter, percentage of pixel intensity over background, and feature circularity. "Ratio of Medians" data were further filtered for 70% present data, Cy5 net median intensity >350 across a minimum of three arrays, Cy3 net median intensity >150 across a minimum of 20 arrays. Expression ratios were $\log_2$ transformed, arrays median centered, quantile normalized, and genes median centered before analysis.

BDGP In Situ Meta-analysis

A table of genes associated with each BDGP anatomical category was generated by downloading and parsing the entire Release 2 website (Tomancak et al., 2002). Stage 13–16 in situ data was compared to 20–24 hr microarray data; other time points from the two studies were incompatible. Replicates in microarray data were averaged by gene and population. For each BDGP category, an average microarray expression value was calculated using data from the genes associated with the category. Categories with fewer than five associated genes were removed. For each category-population pair, a random background distribution was generated by iteratively (10,000 repetitions) retrieving expression data for a set of randomly selected probes equivalent in number to the true associated probes. Appropriateness of normal distribution fitting was assessed by the Kolmogorov-Smirnov goodness of fit test, and a Z score and associated p value for the observed expression mean relative to the random background distribution was calculated for every category-population pair. Data were visualized as a bubble plot in which in situ categories and microarray populations were organized by hierarchical clustering using a correlation distance metric. Categories were color coded as in Tomancak et al. (2007).

Identification of Differentially Regulated Genes

Differentially expressed genes were identified using Significance Analysis for Microarrays (Tusher et al., 2001). Pairwise comparisons were performed with a fold change threshold of 1.5 or 2.0 and false discovery rate of 1%. Hierarchical clustering and heatmap visualization were performed as previously described (Kim et al., 2012).

Regulatory Network Modeling

Our custom expression array targeted multiple isoforms per gene and frequently multiple probes per isoform. To reduce complexity for network modeling, we averaged probe values

if their correlations were greater than 0.6 across all samples. Probe-averaged transcript groups were used for information theoretic regulatory network modeling. The network was based on mutual information as implemented in ARACNE (Margolin et al., 2006). Statistical thresholding was applied at $p = 10^{-7}$, and the data processing inequality applied with $e = 0.10$. Networks were visualized using Cytoscape.

Quantitative Real-Time PCR

RNA was isolated from 40 dissected VNC preparations using the Direct-zol RNA miniprep kit (Zymo Research), reverse transcribed into cDNA, and transcript levels quantified in SYBR Select (Life Technologies) on an ABI StepOne Plus instrument (Life Technologies). Primers used were rpl32f, 5′-CAGATACTGTCCCTTGAAGCG-3′; rpl32r, 5′-TGGCTTCTGTTTGTGATGGG-3′; krF, 5′-GTGTGCGGGAAAACATTGC-3′; and krR, 5′-CAGAAGTTGGGTAGGTGAGAG-3′. Data were analyzed by the Pfaffl method.

Microscopy

Microscopy was performed as previously described (Bergquist et al., 2010; Parrish et al., 2007). Embryos were fixed in a 1:1 mixture of heptane: 4% formaldehyde, devitellinized in methanol, and washed extensively in PBS-Tx (0.2% Triton X-100) prior to immunostaining. Larval tissue was fixed in 4% EM-grade formaldehyde (EM sciences) for 30–60 min at room temperature and then washed extensively in PBS-Tx. Samples were blocked for 30 min in 5% normal donkey serum, incubated with primary antibody overnight at 4°C, washed, and incubated in secondary antibodies (Jackson Laboratory) prior to mounting in Vecta-shield (Vector Laboratories) or dehydration and mounting of fillets in DPX (Leica) and imaging on a Leica SP2 or SP5 confocal microscope. Antibodies were as follows: guinea anti-Kr, 1:2,000 (Kosman et al., 1998); 22C10, 1:800 (Developmental Studies Hybridoma Bank); mouse anti-GFP 1:1,000 (Life Technologies). Alexa-conjugated secondary antibodies and FITC-conjugated goat anti-HRP were used at 1:250 (Jackson ImmunoResearch Laboratories).

Electrophysiology

Recordings were made from muscle 6 in abdominal segments 2 and 3 from third-instar larvae, as previously described (Frank et al., 2006, 2009). Recordings were made in HL3 saline containing 70 mM NaCl, 5 mM KCl, 10 mM $MgCl_2$, 10 mM $NaHCO_3$, 115 mM sucrose, 4.2 mM trehalose, 5 mM HEPES, and 0.3 mM $CaCl_2$. Quantal content was calculated by dividing the average EPSP amplitude by the average mEPSP amplitude, for each muscle recording. For acute pharmacological homeostatic challenge, larvae were incubated in Philanthotoxin-433 (PhTx; 10–20 μM; Sigma-Aldrich) for 10 min (Frank et al., 2006).

Supplementary Material

Refer to Web version on PubMed Central for supplementary material.

Acknowledgments

REFERENCES

Adryan B, Teichmann SA. FlyTF: a systematic review of site-specific transcription factors in the fruit fly Drosophila melanogaster. Bioinformatics. 2006; 22:1532–1533. [PubMed: 16613907]

Bergquist S, Dickman DK, Davis GW. A hierarchy of cell intrinsic and target-derived homeostatic signaling. Neuron. 2010; 66:220–234. [PubMed: 20434999]

Bozdech Z, Zhu J, Joachimiak MP, Cohen FE, Pulliam B, DeRisi JL. Expression profiling of the schizont and trophozoite stages of Plasmodium falciparum with a long-oligonucleotide microarray. Genome Biol. 2003; 4:R9. [PubMed: 12620119]

Davis GW. Homeostatic control of neural activity: from phenomenology to molecular design. Annu. Rev. Neurosci. 2006; 29:307–323. [PubMed: 16776588]

Driscoll HE, Muraro NI, He M, Baines RA. Pumilio-2 regulates translation of Nav1.6 to mediate homeostasis of membrane excitability. J. Neurosci. 2013; 33:9644–9654. [PubMed: 23739961]

Dulcis D, Jamshidi P, Leutgeb S, Spitzer NC. Neurotransmitter switching in the adult brain regulates behavior. Science. 2013; 340:449–453. [PubMed: 23620046]

Frank CA, Kennedy MJ, Goold CP, Marek KW, Davis GW. Mechanisms underlying the rapid induction and sustained expression of synaptic homeostasis. Neuron. 2006; 52:663–677. [PubMed: 17114050]

Frank CA, Pielage J, Davis GW. A presynaptic homeostatic signaling system composed of the Eph receptor, ephexin, Cdc42, and CaV2.1 calcium channels. Neuron. 2009; 61:556–569. [PubMed: 19249276]

Gho M, Ganetzky B. Analysis of repolarization of presynaptic motor terminals in Drosophila larvae using potassium-channel-blocking drugs and mutations. J. Exp. Biol. 1992; 170:93–111. [PubMed: 1328458]

Hoch M, Jäckle H. Krüppel acts as a developmental switch gene that mediates Notch signalling-dependent tip cell differentiation in the excretory organs of Drosophila. EMBO J. 1998; 17:5766–5775. [PubMed: 9755176]

Houweling AR, Bazhenov M, Timofeev I, Steriade M, Sejnowski TJ. Homeostatic synaptic plasticity can explain post-traumatic epilepto-genesis in chronically isolated neocortex. Cereb. Cortex. 2005; 15:834–845. [PubMed: 15483049]

Isshiki T, Pearson B, Holbrook S, Doe CQ. Drosophila neuroblasts sequentially express transcription factors which specify the temporal identity of their neuronal progeny. Cell. 2001; 106:511–521. [PubMed: 11525736]

Jiang J, Chan Y-S, Loh Y-H, Cai J, Tong G-Q, Lim C-A, Robson P, Zhong S, Ng H-H. A core Klf circuitry regulates self-renewal of embryonic stem cells. Nat. Cell Biol. 2008; 10:353–360. [PubMed: 18264089]

Kim CC, Nelson CS, Wilson EB, Hou B, DeFranco AL, DeRisi JL. Splenic red pulp macrophages produce type I interferons as early sentinels of malaria infection but are dispensable for control. PLoS ONE. 2012; 7:e48126. [PubMed: 23144737]

Kosman D, Small S, Reinitz J. Rapid preparation of a panel of polyclonal antibodies to Drosophila segmentation proteins. Dev. Genes Evol. 1998; 208:290–294. [PubMed: 9683745]

MacLean JN, Zhang Y, Goeritz ML, Casey R, Oliva R, Guckenheimer J, Harris-Warrick RM. Activity-independent coregulation of IA and Ih in rhythmically active neurons. J. Neurophysiol. 2005; 94:3601–3617. [PubMed: 16049145]

Marder E, Goaillard J-M. Variability, compensation and homeostasis in neuron and network function. Nat. Rev. Neurosci. 2006; 7:563–574. [PubMed: 16791145]

Margolin AA, Nemenman I, Basso K, Wiggins C, Stolovitzky G, Dalla Favera R, Califano A. ARACNE: an algorithm for the reconstruction of gene regulatory networks in a mammalian cellular context. BMC Bioinformatics. 2006; 7(Suppl 1):S7. [PubMed: 16723010]

Marygold SJ, Leyland PC, Seal RL, Goodman JL, Thurmond J, Strelets VB, Wilson RJ. FlyBase consortium. FlyBase: improvements to the bibliography. Nucleic Acids Res. 2013; 41(Database issue):D751–D757. [PubMed: 23125371]

Mee CJ, Pym ECG, Moffat KG, Baines RA. Regulation of neuronal excitability through pumilio-dependent control of a sodium channel gene. J. Neurosci. 2004; 24:8695–8703. [PubMed: 15470135]

Moore DL, Blackmore MG, Hu Y, Kaestner KH, Bixby JL, Lemmon VP, Goldberg JL. KLF family members regulate intrinsic axon regeneration ability. Science. 2009; 326:298–301. [PubMed: 19815778]

Muraro NI, Weston AJ, Gerber AP, Luschnig S, Moffat KG, Baines RA. Pumilio binds para mRNA and requires Nanos and Brat to regulate sodium current in Drosophila motoneurons. J. Neurosci. 2008; 28:2099–2109. [PubMed: 18305244]

Nerbonne JM, Gerber BR, Norris A, Burkhalter A. Electrical remodelling maintains firing properties in cortical pyramidal neurons lacking KCND2-encoded A-type K+ currents. J. Physiol. 2008; 586:1565–1579. [PubMed: 18187474]

Parrish JZ, Emoto K, Jan LY, Jan YN. Polycomb genes interact with the tumor suppressor genes hippo and warts in the maintenance of Drosophila sensory neuron dendrites. Genes Dev. 2007; 21:956–972. [PubMed: 17437999]

Ping Y, Tsunoda S. Inactivity-induced increase in nAChRs upregulates ShalK(+) channels to stabilize synaptic potentials. Nat. Neurosci. 2012; 15:90–97. [PubMed: 22081160]

Ramocki MB, Zoghbi HY. Failure of neuronal homeostasis results in common neuropsychiatric phenotypes. Nature. 2008; 455:912–918. [PubMed: 18923513]

Scobie KN, Hall BJ, Wilke SA, Klemenhagen KC, Fujii-Kuriyama Y, Ghosh A, Hen R, Sahay A. Krüppel-like factor 9 is necessary for late-phase neuronal maturation in the developing dentate gyrus and during adult hippocampal neurogenesis. J. Neurosci. 2009; 29:9875–9887. [PubMed: 19657039]

Spitzer NC. Activity-dependent neurotransmitter respecification. Nat. Rev. Neurosci. 2012; 13:94–106. [PubMed: 22251956]

Sur I. Krüppel-like factors 4 and 5: unity in diversity. Curr. Genomics. 2009; 10:594–603. [PubMed: 20514221]

Temporal S, Desai M, Khorkova O, Varghese G, Dai A, Schulz DJ, Golowasch J. Neuromodulation independently determines correlated channel expression and conductance levels in motor neurons of the stomatogastric ganglion. J. Neurophysiol. 2012; 107:718–727. [PubMed: 21994267]

Tomancak P, Beaton A, Weiszmann R, Kwan E, Shu S, Lewis SE, Richards S, Ashburner M, Hartenstein V, Celniker SE, Rubin GM. Systematic determination of patterns of gene expression during Drosophila embryogenesis. Genome Biol. 2002; 3:H0088.

Tomancak P, Berman BP, Beaton A, Weiszmann R, Kwan E, Hartenstein V, Celniker SE, Rubin GM. Global analysis of patterns of gene expression during Drosophila embryogenesis. Genome Biol. 2007; 8:R145. [PubMed: 17645804]

Turrigiano GG, Nelson SB. Homeostatic plasticity in the developing nervous system. Nat. Rev. Neurosci. 2004; 5:97–107. [PubMed: 14735113]

Tusher VG, Tibshirani R, Chu G. Significance analysis of microarrays applied to the ionizing radiation response. Proc. Natl. Acad. Sci. USA. 2001; 98:5116–5121. [PubMed: 11309499]
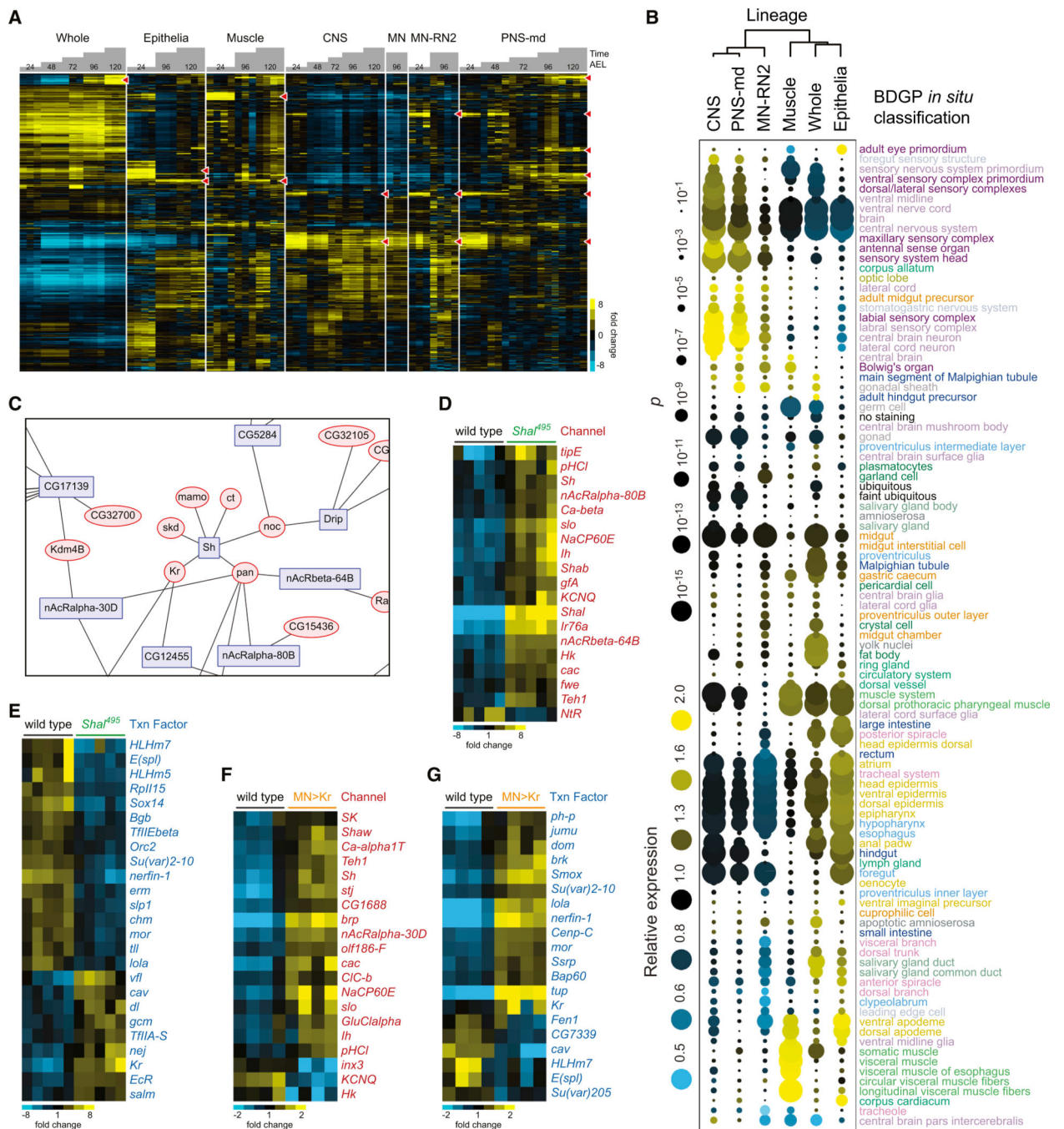
Figure 1. Identification of Kr as a Transcriptional Regulator of Ion Channel Gene Expression
(A) Microarray analysis of isolated cells over development. Genes are organized by
hierarchical clustering (vertical axis) and populations are ordered by developmental time
after egg laying (AEL). Red wedges highlight clusters of developmentally regulated genes.
(B) The mean microarray expression value for all genes associated with each BDGP in situ
category is shown for each population. Bubble color reflects relative expression, and bubble
size represents statistical significance. Categories and populations are hierarchically
clustered, and categories are color coded using the tissue-specific scheme used by Tomancak

et al. (2007). (C) A regulatory network model. Ion channel nodes are depicted as blue rectangles and transcription factors as red ellipses. (D–G) Ion channels (D and F) and a subset of the most statistically significant transcription factors (E and G) differentially regulated in *Shal*[495] mutants (D and E) and motoneurons overexpressing *Kr* (F and G). Columns represent independent samples; fold changes shown are relative to the median expression for a given gene calculated across all depicted samples (D–G).
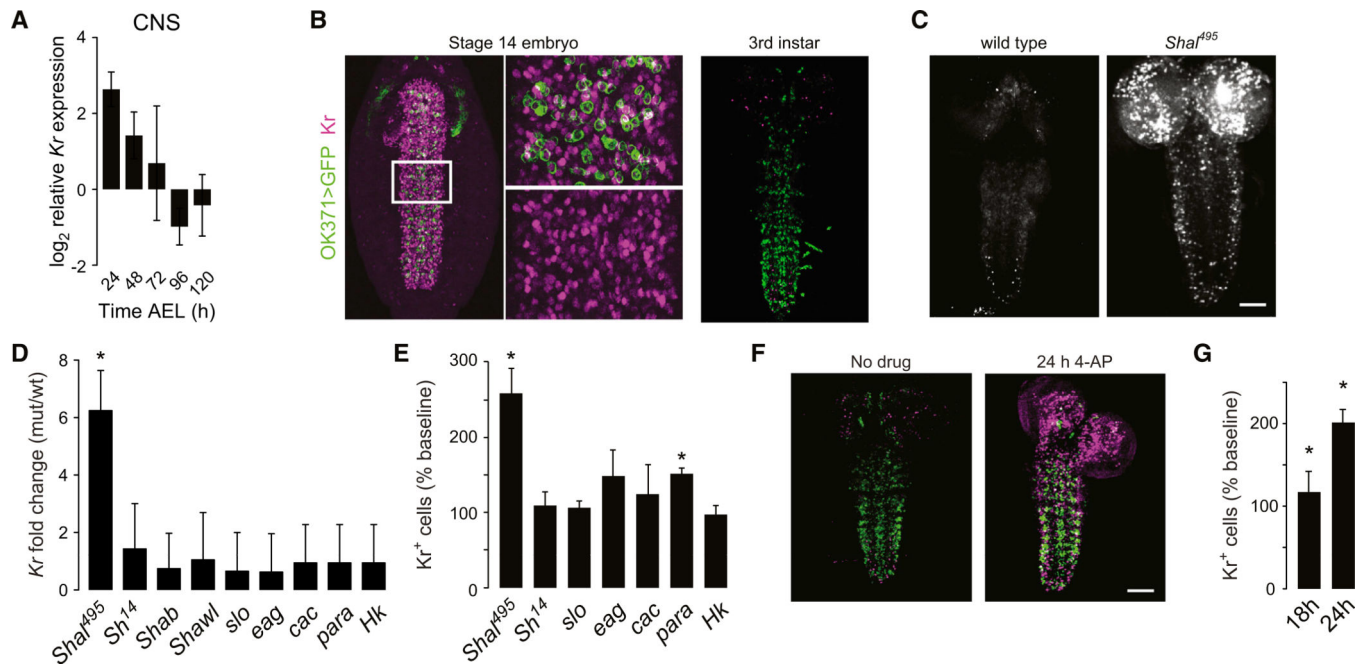
Figure 2. Postembryonic Induction of Kr Is Specific to Loss of *Shal*

(A) *Kr* expression levels during larval development. (B) Kr immunostaining (magenta) in the embryonic (left) and larval (right) CNS. (C) Induction of Kr immunoreactivity in the *Shal* larval nervous system. (D) *Kr* transcript measured by qPCR performed on isolated VNC preparations. (E) Kr staining in ion channel mutants. (F and G) Acute induction of Kr immunostaining (magenta) after 24 hr of 4-AP feeding (F), with (G) quantification of Kr^{+} cells relative to baseline (no drug) (G). *p < 0.05 (D and E, ANOVA with Dunnett's post hoc test; G, t test, 4-AP treated versus mock). Data are presented as mean ± SEM.
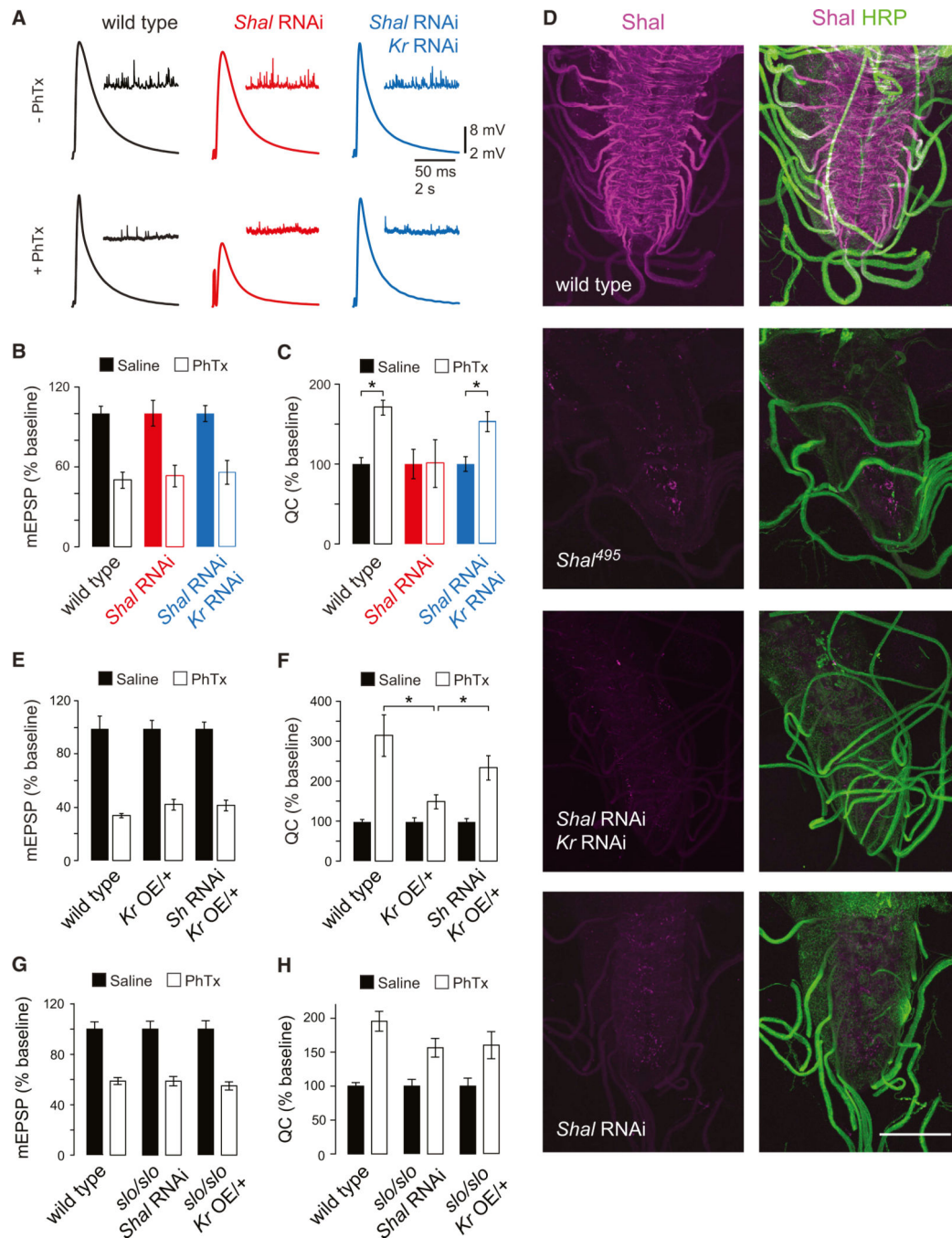
Figure 3. *Kr* Is Necessary and Sufficient for Compensatory Induction of *Sh* Expression
(A) Representative traces for EPSP and mEPSP (inset) amplitudes in the absence (top) or
presence (bottom) of PhTx for wild-type (black), neuronally expressed *Shal-RNAi* (red), and
neuronal coexpression of *Shal-RNAi* with *Kr-RNAi* (blue). (B and C) Quantification of
experiments in (A). Data are normalized to each genotypic background in the absence of
PhTx. (D) Shal immunostaining (magenta) in isolation and colabeled with anti-HRP to label
neuronal membrane (green, right). (E–H) mEPSP amplitudes (E and G) and quantal content

with and without PhTx for the indicated genotypes (F and H). *p < 0.01 (t test). Data are presented as mean ± SEM.
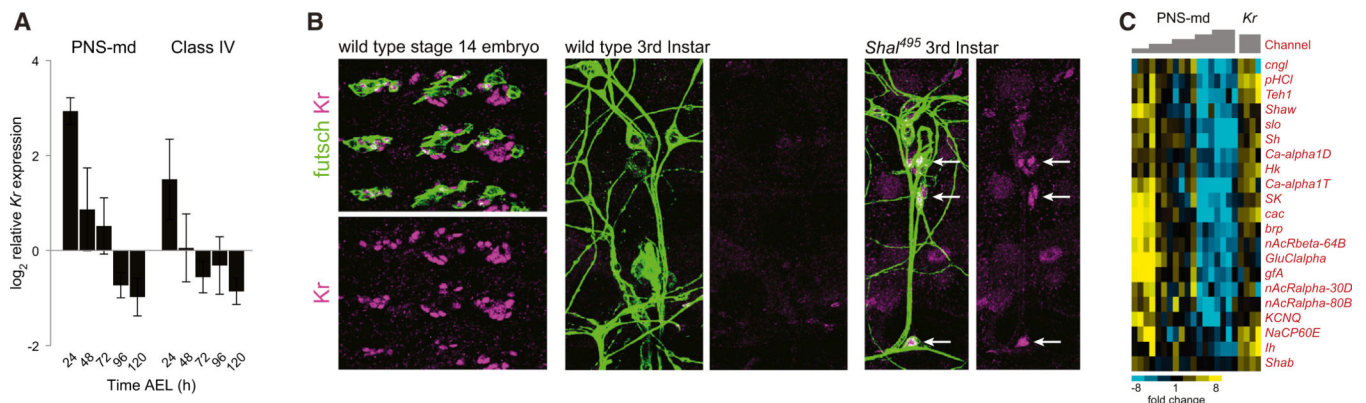
Figure 4. Conserved Expression and Inducibility of Kr in the PNS
(A) *Kr* is expressed embryonically in PNS-md neurons (*Gal4$^{21-7}$ > UAS-mCD8-GFP*) and class IV PNS neurons (*ppk-GFP*) and diminishes over larval development. (B) Kr immunostaining (magenta) in embryonic PNS (left), in third-instar larval PNS (middle), and in *Shal^{495}* PNS (right). Kr levels are 2.5-fold higher than controls in *Shal^{495}* PNS neurons (p = 0.0006, unpaired t test with Welch's correction). Neurons (green) are labeled with anti-*futsch* antibodies (22C10); white arrows indicate Kr$^+$ nuclei of neurons. (C) Channel expression in PNS-md neurons overexpressing *Kr*. Data are presented as mean ± SEM.